Interfacial Tension and Adsorption in the Binary System Ethanol and Carbon Dioxide: Experiments, Molecular Simulation and Density Gradient Theory

Stefan Becker, Stephan Werth, Martin Horsch, Kai Langenbach*, Hans Hasse

Laboratory of Engineering Thermodynamics, University of Kaiserslautern, Erwin-Schrödinger-Strasse 44, 67663 Kaiserslautern, Germany

Abstract

Data on the interfacial tension and adsorption are reported for the binary mixture of ethanol + carbon dioxide (CO_2) as well as for pure ethanol. The data are obtained from experiments, molecular dynamics (MD) simulations, and density gradient theory in combination with the PC–SAFT equation of state (DGT + PC–SAFT). Experimental data of the interfacial tension are reported for 8 temperatures between 303 K and 373 K and pressures up to 6 MPa. The experimental data are compared to results from MD simulations and from DGT + PC–SAFT for which pressures up to 12 MPa are considered. From the experimental data, the relative adsorption of CO_2 is obtained via the Gibbs adsorption equation using the PC–SAFT equation of state. Data on the relative adsorption of CO_2 is also determined both from MD and DGT + PC–SAFT. The three data sets show good agreement. There is a substantial enrichment of CO_2 at the interface. This is consistently predicted both by MD and DGT + PC–SAFT. The work shows that both MD and DGT + PC–SAFT are well suited for detailed studies of interfacial properties and that the independent methods yield similar predictions for those interfacial properties which cannot be studied experimentally.

Keywords: Interfacial Properties, Ethanol + Carbon Dioxide, Experiment, Density Gradient Theory, Molecular Dynamics

*Corresponding author
Email address: (Kai Langenbach)

1. Introduction

The interfacial tension and adsorption play an important role in mass transfer, nucleation, or wetting and, hence, in industrial process design. For pure liquids, numerous experimental data on the interfacial tension are available, whereas for mixtures, the data base is still small [1–3]. Thus, it is desirable to have predictive methods for the description and the characterization of interfacial properties for pure fluids and fluid mixtures. Molecular simulation based on force fields as well as density gradient theory (DGT) in combination with a physically based equation of state (EOS) are very attractive methods for doing this [4–11]. Furthermore, those methods give detailed insight into the properties of the interface on the nanoscale which cannot be obtained experimentally.

In the present work, the interfacial properties of the binary mixture of ethanol and carbon dioxide (CO_2) are examined. There are many experimental studies on the bulk properties of this mixture in vapor–liquid equilibrium [12–19]. Experimental data on the interfacial tension have been reported by Sun and Shekunov [20] and by Dittmar et al. [21, 22], while no information on the interfacial adsorption is available in literature.

Experimental data on the interfacial adsorption can be obtained from the correlation of the interfacial tension with the chemical potential using the Gibbs adsorption equation [23]. Different ways have been used to describe the chemical potential of the adsorbed component. Kahl et al. [24, 25] studied adsorption in binary systems of organic liquids and used the NRTL activity coefficient model [26] for the determination of the chemical potential. For systems of a liquid and a supercritical fluid, for instance, Masterton et al. [27] modeled the chemical potential based on the assumption of the gas phase to consist of pure supercritical fluid. That way, also Mejía et al. [28] recently determined the relative adsorption of CO_2 at the interface of n–decane and n–eicosane. Alternatively, the chemical potential can be obtained from an EOS.

Molecular simulations based on force fields are used here to describe bulk and interfacial properties of the studied mixture. These force fields are parametrized solely based on experimental data of bulk properties. Hence, all results for interfacial properties are predictions. Additionally, the Perturbed–Chain Statistical Associating Fluid Theory (PC–SAFT) EOS is used. Based on a parametrization of PC–SAFT using bulk properties, DGT is applied for describing interfacial properties. Thereby, additional parameters are introduced which are fitted to experimental data of the interfacial tension of the pure compounds ethanol and CO_2. Both theoretical methods have the advantage to give insight into the local properties of

the interfacial region which is presently not obtainable from experiments. In that situation, it is important to have two independent theoretical methods, which is the case here.

Interfacial properties of fluid mixtures were studied by MD simulations or DGT by many authors before, e.g. [10, 11, 29–31, 31–39]. In addition to the interfacial tension, the two methods yield the component density profiles in the interfacial region from which the relative adsorption of a component at the interface can directly be determined [10, 31, 37, 39, 40]. In many mixtures, one of the components shows a maximum of the component density in the interfacial region. We propose here to define enrichment of a component as the ratio of the maximum density of that component in the interfacial region divided by the larger of the bulk densities of the same component.

Pronounced enrichment was found for systems like water + CO_2 [30, 40–42], water + alcohols [11], or N,N-dimethylformamide + alkanes [43] where the maximum local density of the low–boiling component exceeds the liquid bulk density by a factor of more than ten. Low enrichment of less than 1.2 has been observed for mixtures of some hydrocarbons [32, 44].

Mejía et al. [28] recently investigated the interfacial properties of the binary mixtures of CO_2 with n–decane and n–eicosane, respectively, using experiments, the DGT in combination with the SAFT–VR EOS, and MD simulations with coarse grained force fields. They compared the interfacial tension and adsorption data obtained from DGT and MD simulations with the experimental results and good agreement was observed. The maximum relative adsorption of CO_2 in the two systems was on the order of 10 μmol /m^2. An enrichment of CO_2 between two and three was observed.

In the present work, interfacial properties of the binary mixture of ethanol and CO_2 are determined by experimental measurements, MD simulations and the DGT in combination with the PC–SAFT EOS (DGT + PC–SAFT) at temperatures between 303 K and 373 K. The article is organized as follows: The experiments are described in Section 2 and the theoretical methods are introduced in Section 3. In Section 4, the results of the predicted interfacial tension and adsorption are compared with the experimental data. Additionally, the enrichment of CO_2 at the interface is determined and the results obtained from MD simulations and DGT + PC–SAFT are compared. Conclusions are drawn in Section 5. The Appendix contains data on the interfacial tension of pure ethanol as well as further information on the experiments and the MD simulations.

2. Experimental

2.1. Materials

Details of all materials (CAS Number, supplier, purity) are listed in Table 1. Carbon dioxide was used without further purification. Ethanol was degassed by vacuum distillation.

2.2. Pendant drop method for the measurement of interfacial tensions

For the determination of the interfacial tension, the pendant drop method (PDM) [21, 45, 46] is used. The method is based on the mechanical equilibrium of a drop pending at a capillary tube. The mechanical equilibrium which is governed by gravitational forces and the interfacial tension can be described by [45, 46]

$$\gamma \left(\frac{2}{R_{\mathrm{apx}}} - \frac{1}{R_1} - \frac{1}{R_2} \right) = \Delta\rho g z, \tag{1}$$

where γ is the interfacial tension, R_1 and R_2 are the two principal radii of curvature, R_{apx} is the radius of curvature at the apex of the drop, $\Delta\rho = \rho' - \rho''$ is the density difference between the liquid and the vapor phase, g is the gravitational acceleration, and z is the height coordinate of the drop as measured from the apex. From the shape of the drop, the radii of curvature and the height are determined so that the interfacial tension can be calculated from Eq. (1), if appropriate values of the density difference are available. Any error in $\Delta\rho$ will cause a similar error in γ, c.f. Eq. (1). The uncertainty in the interfacial tension measurement using the PDM arises from the uncertainty in the density difference $\Delta\rho$ and from the reproducibility of the measurements which is quantified in Section 4. For the presently studied mixture, $\Delta\rho$ is obtained from the PC–SAFT EOS which is shown to be in good agreement with the available experimental data for $\Delta\rho$, c.f. Appendix A.3.

The PDM yields the interfacial tension as a function of temperature and pressure. By using the PC–SAFT EOS, the mole fraction of CO_2 in the liquid phase x'_{CO_2} at a given temperature and pressure is determined. In that way, the experimental data for the interfacial tension are related to the liquid phase composition.

2.3. Apparatus and procedure

The apparatus used to determine the interfacial tension is shown in Figure 1. The view cell is equipped with two sapphire windows and a magnetic stirrer. It is thermostated by a liquid passing through a jacket. The temperature is measured at two different locations in the thermostated jacket with calibrated platinum resistance thermometers. The accuracy of the temperature measurement is better than

±0.1 K. The pressure is measured with two absolute pressure gauges (WIKA, Germany, 0-25 bar, and 0-100 bar) which are calibrated against a high precision pressure balance (Desgranges et Huot, France, model 5201). The accuracy of the pressure measurement is better than 0.025 bar for pressures less than 25 bar and better than 0.1 bar for higher pressures. The pending drop is formed at a stainless steel capillary with a diameter of 1.571mm. The drop is illuminated by the background light of a diffuse LED luminous field. The drop image is recorded by a CCD–camera (Stingray F-046, Allied Vision Technologies GmbH, Germany) with an objective lens of 70 mm focal length (TELE-XENAR 2.2/70, Jos. Schneider Optische Werke GmbH, Germany). The processing of the drop image and the determination of the interfacial tension is accomplished at a PC (Software DSA1 vs. 1.92.1, Krüss, Germany).

The procedure of measuring the interfacial tension is described in the following. Prior to a measurement, the chamber and the connected lines are rinsed with acetone from a liquid reservoir. Then the apparatus is rinsed with pure ethanol twice. Subsequently, the entire apparatus is evacuated.

For measurements in the binary system of ethanol and CO_2, ethanol is degassed and filled into the evacuated and thermostated view cell with a hand pump so that a liquid reservoir forms at the bottom of the view cell. Subsequently, CO_2 is filled into the view cell from a reservoir container. The pressure in the chamber is adjusted by the amount of CO_2 added. For the enhancement of the equilibration, the cell content is stirred with a magnetic stirrer. During equilibration, the stirred mixture is continuously recirculated with a thermostated dosing pump (HPD Pump Multitherm 200, Bischoff, Germany). After the equilibration, the dosing pump is stopped. Via the needle valve, a small portion of the mixed liquid is displaced so that a drop is formed at the capillary. The drop image is taken after complete equilibration about 15 minutes after the drop is formed.

The uncertainty in the interfacial tension data that stems from the uncertainty in $\Delta\rho$ is up to 0.6 %, c.f. Section A.3. The random uncertainty of measurement method was determined from repeated measurements of the interfacial tension of pure ethanol, where the entire temperature range is covered. For further details see Appendix A.1. The random uncertainty of the measurement method is less than 1.3 % and the total uncertainty in the experimental data on the interfacial tension of the binary mixture is better than 1.9 %.

The procedure for measurements of the interfacial tension of pure ethanol is analogue and described in the Appendix A.1.

2.4. Determination of the relative adsorption from experimental data of the interfacial tension

The adsorption of CO_2 at the interface $\Gamma_{CO_2}^{(EtOH)}$ relative to ethanol(EtOH) is determined from the Gibbs adsorption equation [23]

$$\Gamma_{CO_2}^{(EtOH)} = -\left.\frac{\partial\gamma}{\partial\mu_{CO_2}}\right|_T = -\left.\frac{f''_{CO_2}}{RT}\frac{\partial\gamma}{\partial f''_{CO_2}}\right|_T , \tag{2}$$

where the chemical potential of CO_2 at saturation μ_{CO_2} is expressed here by the fugacity of CO_2 in the vapor phase $f''_{CO_2} = px''_{CO_2}\phi''_{CO_2}$, with the fugacity coefficient ϕ''_{CO_2}. The fugacity is calculated by the PC–SAFT EOS at every state point (characterized by (T, p)) at which the interfacial tension is measured. A value of the fugacity f''_{CO_2} is assigned to each value of the experimentally determined interfacial tension. A polynomial is fitted to the pairs (γ, f''_{CO_2}) along an isotherm and from this polynomial the derivative in Eq. (2) is obtained. The adsorption data obtained that way are referred to as experimental data, in the following.

3. Modelling and simulation

3.1. Interfacial Adsorption, Density Profiles and Enrichment

The MD simulations and the DGT + PC–SAFT yield the component density profiles $\rho_i(y)$ of both CO_2 and ethanol in the interfacial region. On the basis of the density profile, the relative adsorption of CO_2 is computed via the symmetric interface segregation introduced by Wadewitz and Winkelmann [47]

$$\Gamma_{CO_2}^{(EtOH)} = -\left(\rho'_{CO_2} - \rho''_{CO_2}\right) \int_{-\infty}^{\infty} \left[\frac{\rho_{EtOH}(y) - \rho'_{EtOH}}{\rho'_{EtOH} - \rho''_{EtOH}} - \frac{\rho_{CO_2}(y) - \rho'_{CO_2}}{\rho'_{CO_2} - \rho''_{CO_2}} \right] \mathrm{d}y, \quad (3)$$

where ρ'_i and ρ''_i are the component densities at saturation in the bulk liquid and bulk vapor phase, respectively.

Another way to characterize the interfacial excess is the interfacial enrichment E, which is defined in the present work as the ratio between the maximum local component density of CO_2 in the interfacial region and the larger of the component densities of CO_2 in the two bulk phases, which corresponds to the liquid phase in the present work.

$$E_{CO_2} = \frac{\max(\rho_{CO_2}(y))}{\max\left(\rho'_{CO_2}, \rho''_{CO_2}\right)}, \quad (4)$$

By definition, the enrichment assumes values equal to or larger than unity. The adsorption and the enrichment are linked, but do not express the same information. Adsorption may occur if there is no enrichment ($E_{CO_2} = 1$), but an enrichment will generally result in an adsorption.

3.2. Molecular Model and Simulation Method

The molecular model for CO_2 is taken from Merker et al. [48]. It is build of three Lennard-Jones sites, representing each atom and a point quadrupole in the center of mass. The ethanol model is taken from Schnabel et al. [49] and consists of three Lennard-Jones sites (for the methylene, the methyl, and the hydroxyl group) and three partial charges, to account for polarity as well as hydrogen bonding [50, 51]. The molecular models are rigid. The potential energy is given by

$$U = \sum_{i=1}^{N-1} \sum_{j=i+1}^{N} \left\{ \sum_{a=1}^{n_i^{\mathrm{LJ}}} \sum_{b=1}^{n_j^{\mathrm{LJ}}} 4\varepsilon_{ijab} \left[\left(\frac{\sigma_{ijab}}{r_{ijab}} \right)^{12} - \left(\frac{\sigma_{ijab}}{r_{ijab}} \right)^{6} \right] + \sum_{c=1}^{n_i^{e}} \sum_{d=1}^{n_j^{e}} \frac{1}{4\pi\varepsilon_0} \left[\frac{q_{ic} q_{jd}}{r_{ijcd}} + \frac{q_{ic} Q_{jd} + q_{jd} Q_{ic}}{r_{ijcd}^3} \cdot f_1(\omega_i, \omega_j) + \frac{Q_{ic} Q_{jd}}{r_{ijcd}^5} \cdot f_2(\omega_i, \omega_j) \right] \right\}, \tag{5}$$

where ε_{ijab} and σ_{ijab} are the Lennard-Jones energy and size parameter, r_{ijab} and r_{ijcd} are site-site distances, q_{ic}, q_{jd}, Q_{ic} and Q_{jd} are the magnitude of the electrostatic interactions, i.e. the point charges, quadrupole moments, and $f_{\mathrm{k}}(\omega_i, \omega_j)$ are dimensionless angle-dependent expressions in terms of the orientation ω_i,ω_j of the point multipoles [52].

The unlike electrostatic interactions, e.g. between charges and quadrupoles, are treated in a physically straightforward way, following the laws of electrostatics. The modified Lorentz-Berthelot combining rules are used [53, 54] for the interaction between unlike Lennard-Jones sites

$$\sigma_{ij} = \frac{\sigma_{ii} + \sigma_{jj}}{2}, \tag{6}$$

$$\varepsilon_{ij} = \xi \sqrt{\varepsilon_{ii} \varepsilon_{jj}}. \tag{7}$$

The parameters of the molecular models of the pure components which are used here [48, 49] were adjusted to reproduce the saturated liquid density, the vapor pressure and the enthalpy of vaporization. The relative mean deviations between the calculated values by the molecular simulation and experimental data are 0.3 %, 3.7 % and 0.9 % for ethanol [55] and 0.4 %, 1.8 % and 8.1 % for carbon dioxide [48]. The surface tension was not considered in the parametrization of the molecular models. For other pure fluids with a similar parametrization strategy the surface tension is usually overestimated by about 20 % [56–68]. The binary interaction parameter ξ is fitted to experimental data of the vapor-liquid equilibrium of the mixture of ethanol + CO_2 at 333.2 K [18], resulting in $\xi = 1.08$. For a discussion see Section 4.1.

For the present series of molecular dynamics simulations, systems were considered where the vapor and liquid phases coexist with each other in direct contact, employing periodic boundary conditions, so that there are two vapor-liquid interfaces which are oriented perpendicular to the y axis. The surface tension was

computed from the deviation between the normal and the tangential diagonal components of the overall pressure tensor[69, 70], i.e. the mechanical route

$$\gamma = \frac{1}{2}\int_{-\infty}^{\infty} \mathrm{d}y \left(p_\mathrm{N} - p_\mathrm{T}\right). \tag{8}$$

Thereby, the normal pressure p_N is given by the y component of the diagonal of the pressure tensor, and the tangential pressure p_T was determined by averaging over x and z components of the diagonal of the pressure tensor. Further details on the MD simulations are given in the Appendix B.1 .

3.3. Density gradient theory with PC-SAFT EOS

3.3.1. Density gradient theory

Using density gradient theory, originally introduced by van der Waals [71], later rediscovered by Cahn and Hilliard [72] for pure compounds, then generalized to mixtures by Poser and Sanchez [44] and simplified for multi-component mixtures by Miqueu et al. [73], the interfacial tension of mixtures in VLE can be calculated as [73]

$$\gamma = \int_{\rho'_\mathrm{ref}}^{\rho''_\mathrm{ref}} \sqrt{2\Delta\Omega(\boldsymbol{\rho}) \sum_i \sum_j \kappa_{ij} \frac{\mathrm{d}\rho_i}{\mathrm{d}\rho_\mathrm{ref}} \frac{\mathrm{d}\rho_j}{\mathrm{d}\rho_\mathrm{ref}}} \quad \mathrm{d}\rho_\mathrm{ref}, \tag{9}$$

where $\boldsymbol{\rho}$ is the vector of molar component densities, ρ_i and ρ_j are the molar component densities of component i and j respectively, κ_{ij} is the so-called influence parameter of the component pair i and j , $\Delta\Omega(\boldsymbol{\rho}) = a_0(\boldsymbol{\rho}) - \sum_i \rho_i \mu_i^\mathrm{bulk} + p^\mathrm{S}$ is the grand potential per volume, with $a_0(\boldsymbol{\rho})$ being the homogenous free energy per volume at the local density vector, μ_i^bulk is the saturated bulk phase chemical potential of component i and p^S is the pressure at saturation, ρ_ref is a suitably chosen reference density, which is the density of the high boiling component ethanol in our case. The summations run over all components and the integration is between the reference density at saturation in the vapor phase ρ''_ref and the liquid phase ρ'_ref.

The position in the interface as a function of the reference density is calculated with [73]

$$\int_{y_0}^{y} \mathrm{d}y = \int_{\rho^0_\mathrm{ref}}^{\rho_\mathrm{ref}(y)} \sqrt{\Delta\Omega^{-1}(\boldsymbol{\rho}) \sum_i \sum_j \frac{1}{2}\kappa_{ij} \frac{\mathrm{d}\rho_i}{\mathrm{d}\rho_\mathrm{ref}} \frac{\mathrm{d}\rho_j}{\mathrm{d}\rho_\mathrm{ref}}} \quad \mathrm{d}\rho_\mathrm{ref}, \tag{10}$$

where ρ^0_ref is an arbitrarily chosen reference density at the position $y = 0$ between the liquid and vapor densities of the reference component. For the remainder of this article we choose $\rho^0_\mathrm{ref} = 0.5(\rho'_\mathrm{ref} + \rho''_\mathrm{ref})$.

For the evaluation of Eq. (9) and (10), $\boldsymbol{\rho}$ has to be known as a function of ρ_{ref}. That is in this case, we need $\rho_{\mathrm{CO_2}}\left(\rho_{\mathrm{EtOH}}\right)$. We assume here, that the mixed influence parameter $\kappa_{\mathrm{EtOH,CO_2}}$ is calculated from the geometrical mixing rule

$$\kappa_{\mathrm{EtOH,CO_2}} = \sqrt{\kappa_{\mathrm{EtOH,EtOH}}\,\kappa_{\mathrm{CO_2,CO_2}}}. \tag{11}$$

Hence, the relation between component densities is obtained from [73]

$$\sqrt{\kappa_{\mathrm{CO_2,CO_2}}}\,\Delta\mu_{\mathrm{EtOH}}(\boldsymbol{\rho}) = \sqrt{\kappa_{\mathrm{EtOH,EtOH}}}\,\Delta\mu_{\mathrm{CO_2}}(\boldsymbol{\rho}), \tag{12}$$

where $\Delta\mu_i = \mu_i(\boldsymbol{\rho}) - \mu_i^{\mathrm{bulk}}$ is the difference between the chemical potential μ_i at the density vector $\boldsymbol{\rho}$ and the chemical potential at bulk conditions μ_i^{bulk}, calculated from the PC–SAFT EOS here. Here, $\kappa_{\mathrm{CO_2,CO_2}} = 2.5435 \cdot 10^{-20}\ \mathrm{Jm^5/mol^2}$ is taken from the literature [74] and $\kappa_{\mathrm{EtOH,EtOH}}$ is fitted to data on the interfacial tension of pure ethanol resulting in

$$\kappa_{\mathrm{EtOH,EtOH}} \cdot 10^{20}\frac{\mathrm{mol^2}}{\mathrm{Jm^5}} = \frac{T}{99.06\ \mathrm{K}} + 2.2828. \tag{13}$$

We chose here to use a temperature dependent influence parameter for performance reasons. Leaving this parameter constant does, however, only have minor influences in the desired temperature range.

3.3.2. PC–SAFT EOS

In this work, the PC-SAFT [8, 9] is used as the EOS. The details of the EOS are described elsewhere [8, 9]. For non-associating compounds, the PC-SAFT equation of state has three pure compound parameters, the segment number m, the segment diameter σ and the segment-segment interaction energy ε. For associating compound, also the association volume κ^{AB} and the association energy ε^{AB} between two association sites A and B is necessary. Furthermore, in this case the number of association sites of the different types (here proton donor, n_P, electron donor, n_E) has to be specified [75]. Pure component parameters for ethanol and CO_2 are taken from the literature [8, 9, 76]. We refrain here from using the quadrupolar CO_2 model of Gross [77], even though it is known to give excellent results for the pure component properties. But taking it into a mixture with ethanol in a meaningful way would require a polar and associating ethanol model, which is presently not available. CO_2 is modeled as a compound that does not form self–associates. However, it is allowed to cross-associate with ethanol. For this case, Kleiner and Sadowski [76] give the cross–association energy

$$\varepsilon^{\mathrm{AB}}_{\mathrm{CO_2,EtOH}} = \frac{1}{2}\varepsilon^{\mathrm{AB}}_{\mathrm{EtOH,EtOH}} \tag{14}$$

and cross–association volume

$$\kappa^{\mathrm{AB}}_{\mathrm{CO_2,EtOH}} = \kappa^{\mathrm{AB}}_{\mathrm{EtOH,EtOH}} \left(2 \frac{\sqrt{\sigma_{\mathrm{CO_2,CO_2}}\, \sigma_{\mathrm{EtOH,EtOH}}}}{\sigma_{\mathrm{CO_2,CO_2}} + \sigma_{\mathrm{EtOH,EtOH}}} \right) \tag{15}$$

Parameters and references for literature data are given in Table 2.

Aside from the pure compound parameters, there is the binary parameter k_{ij} for the binary mixture from the modified Berthelot combining rule

$$\varepsilon_{ij} = (1 - k_{ij}) \sqrt{\varepsilon_{ii} \varepsilon_{jj}}. \tag{16}$$

The Lorentz combining rule, Eq. (6), is applied for the segement size parameter σ_{ij}. The parameter $k_{\mathrm{CO_2,EtOH}}$ for the binary system of ethanol + CO_2 is fitted to experimental data of the vapor–liquid equilibrium [16–18]. A temperature dependent correlation for $k_{\mathrm{CO_2,EtOH}} = 7.5064\ \mathrm{K} \ / \ T + 0.0545$ is obtained. For a discussion see Section 4.1.

4. Results and discussion

4.1. Vapor–liquid equilibrium of the binary system ethanol + CO_2

The composition of the liquid and the vapor phase at saturation is described with the PC–SAFT EOS and with MD simulations. Figure 2 shows the results from MD simulations and the PC–SAFT EOS for the vapor–liquid equilibrium of the binary mixture at 303.2 K, 333.2 K, and 363.2 K. Experimental data on the vapor–liquid equilibrium of the binary mixture are available at 303.2 K and about 333.5 K, but not at 363.2 K. At 303.2 K, the experimental data are well represented both by MD simulations and by PC–SAFT. At 333.2 K, the PC–SAFT EOS overestimates the critical pressure of the mixture which is an often observed deficiency of EOSs. Nevertheless, the PC–SAFT and the MD simulation results show overall good agreement with the experimental data of the vapor–liquid equilibrium.

[Figure 2 about here]

4.2. Interfacial tension of the binary mixture of ethanol and CO_2

In the binary system ethanol + CO_2, the interfacial tension is experimentally determined at 8 temperatures between 303.2 K and 373.2 K and pressures up to 6 MPa. The experimental results are listed in Table 3. In Figure 3, two isotherms of the interfacial tension are plotted versus pressure. It can be seen that the interfacial tension γ decreases with increasing pressure at a given temperature. At low pressures, γ decreases with temperature and at pressures above about 4 bar, the opposite trend is observed, i.e. the interfacial tension rises with pressure. The experimental data of the present work are compared to the experimental data of Dittmar et al. [21, 22] at temperatures of about 303.5 K and 323.5 K. Good agreement between the two data sets is observed, c.f. Figure 3.

[Table 3 and Figure 3 about here]

The DGT + PC–SAFT results agree well with the present experimental data. The average absolute deviation is 4.6 % over the entire temperature and pressure range. The MD simulation results overestimate the interfacial tension in the binary mixture by a constant factor of about 25 % in the entire temperature and pressure range which is ascribed to the deviation of the molecular model for pure ethanol from the interfacial tension of the pure component. To study the influence of CO_2 on the interfacial tension of the binary mixture, the reduced interfacial tension γ^{red} is introduced by

$$\gamma^{\mathrm{red}} = \frac{\gamma}{\gamma^{\mathrm{pure}}}, \tag{17}$$

where γ^{pure} is the interfacial tension of pure ethanol at the same temperature. Figure 4 shows three isotherms of the reduced interfacial tension of the binary mixture of ethanol and CO_2 over the mole fraction of CO_2 in the liquid phase. The interfacial tension decreases non-linearly with the mole fraction of CO_2 in the liquid phase. A good agreement between DGT + PC–SAFT, MD simulation and the experimental data is found for all three isotherms.

[Figure 4 about here]

4.3. Interfacial adsorption and enrichment

Figure 5 shows the density profiles of the two components ethanol and CO_2 in the interfacial region at temperatures of 303.2 K, 333.2 K, and 363.2 K and mole fractions of CO_2 in the liquid phase of 0.29 mol/mol, 0.27 mol/mol, and 0.25 mol/mol, respectively. The component density of ethanol increases monotonously from the vapor to the liquid phase, whereas the component density of carbon dioxide shows a maximum at the interface. With increasing temperature, the width of the interfacial region increases, as expected, and the maximum in the component density profile of CO_2 is less pronounced. The MD simulations and DGT + PC–SAFT show a similar behavior. The MD simulations, however, predict a larger interfacial width and a smaller maximum of the component density of CO_2 as compared to the prediction by DGT + PC–SAFT. This is ascribed to the interfacial fluctuations which are present in the MD simulation, whereas the DGT + PC–SAFT model assumes a perfectly flat interface. It might, however, also be partly due to the different methods used.

[Figure 5 about here]

The interfacial excess of CO_2 is characterized in the following by two quantities: the relative adsorption and the enrichment at the interface.

From the experimental data of the interfacial tension, the relative adsorption of CO_2 at the interface $\Gamma_{CO_2}^{(EtOH)}$ is obtained from Eq. (2) in combination the PC–SAFT EOS. Using DGT + PC–SAFT and the MD simulation, the relative adsorption $\Gamma_{CO_2}^{(EtOH)}$ is directly obtained from the density profile, using Eq. (3). The results on the relative adsorption are shown in Figure 6. The relative adsorption is higher at lower temperatures and a strong dependence of the relative adsorption of CO_2 on the mole fraction of CO_2 in the liquid phase can be observed. The relative adsorption increases with x'_{CO_2} to a maximum and a further increase of x'_{CO_2} leads to a depletion of the relative adsorption such that at the critical point of the mixture, the relative adsorption is zero. The experimental and MD simulation data show consistently a maximum of the interfacial adsorption of CO_2 of about 15 μmol/m^2 at 303.2 K. At that temperature, the DGT + PC–SAFT results are only shown in part,

as the region in close vicinity to the critical point of CO_2 is not represented well. Except for the vicinity to the mixture critical point at 303.2 K, the experimental data and the DGT + PC–SAFT results agree within about 10 %. On average, the MD simulation results for the relative adsorption deviate by about 40 % from the data of the two other methods. Overall, all three methods qualitatively agree with each other.

[Figure 6 about here]

The enrichment can solely be determined by the component density profiles which are obtained from DGT + PC–SAFT and the MD simulations. Figure 7 shows the enrichment of CO_2 at the interface at temperatures of 303.2 K, 333.2 K, and 363.2 K. Both methods predict a maximum density of CO_2 at the interface that is up to about three times higher than the corresponding density in the liquid phase. The enrichment decreases with increasing temperature and with increasing mole fraction of CO_2 in the liquid phase. Close to the mixture critical point, the enrichment approaches unity. While both methods agree qualitatively, the enrichment determined from MD simulations is consistently lower than the enrichment determined from DGT +PC–SAFT, except maybe for very low concentrations of CO_2 in the liquid phase.

[Figure 7 about here]

5. Conclusion

The interfacial properties of the binary mixture of ethanol and CO_2 were investigated experimentally, by MD simulation and by DGT + PC–SAFT. The experimental data on the interfacial tension and the results of DGT + PC–SAFT agree well for pure ethanol and for the binary mixture. The molecular model of ethanol overestimates the interfacial tension of pure ethanol. As a consequence, the MD simulations also yield interfacial tension data of the binary mixture of ethanol + CO_2 that are larger than the experimental data. The influence of the addition of CO_2 on the interfacial tension is, however, very well predicted by the MD simulation. This is shown by using the reduced interfacial tension, which is the interfacial tension of the mixture divided by that of pure ethanol.

The data for the relative interfacial adsorption of CO_2 that were obtained experimentally, from MD simulations, and from DGT + PC–SAFT show good qualitative agreement. The relative adsorption of CO_2 increases with increasing mole fraction of CO_2 in the liquid phase to a maximum of about 15 μmol/m^2 and on approach to the critical point of the mixture it decreases to zero. The relative adsorption is most pronounced at low temperatures.

The component density profiles that are obtained from MD simulations and DGT + PC–SAFT exhibit enrichment of CO_2 at the interface. The enrichment of CO_2 is defined in the present work as the ratio of the maximum density of CO_2 in the interfacial region divided by the larger of the bulk densities of CO_2. The results of both methods consistently show an enrichment of CO_2 at the interface of up to 3. The enrichment lowers with increasing mole fraction of CO_2 in the liquid phase and with increasing temperature. Over the entire range of temperatures and pressures studied here, the agreement of the two predictions is good.

The work shows that both MD and DGT + PC–SAFT are well suited for detailed studies of interfacial properties and that the independent methods yield similar predictions for the interfacial properties which cannot be studied experimentally.

A. Experimental

A.1. Measurements of the interfacial tension of pure ethanol

For the determination of the interfacial tension of pure ethanol, the density of the liquid phase was calculated with the EOS according to Dillon and Penoncello [78]. The vapor phase density was calculated with the ideal gas law, as the vapor pressure of ethanol does not exceed 2.5 bar at the temperatures which are of interest here.

Before the measurement, the liquid is degassed and filled into the evacuated and thermostated view cell with the hand pump so that a liquid reservoir forms at the bottom of the chamber. Then, via the needle valve, some more liquid is displaced so that a drop forms at the capillary. As the drop is initially heating up in the measuring chamber, the drop image is taken after a steady state is reached which is about 15 minutes after the formation of the drop.

Each measurement was repeated three times to determine the reproducibility of the method. The agreement between the three measurements is good: For any temperature, the three values of the interfacial tension differ less than 1.3 %. A systematic uncertainty in the experimental data of the interfacial tension arises from the uncertainty in the saturated density difference between the liquid and the vapor phase $\Delta\rho$. This contribution to the uncertainty of the interfacial tension is less than 0.2 % [78]. The overall uncertainty of the present experimental data for pure ethanol is about 1.5 %.

A.2. Data of the interfacial tension of pure ethanol

The interfacial tension of pure ethanol is measured at temperatures between 303.2 K and 373.2 K. The experimental results are listed in Table A.1. Figure A.1 shows the interfacial tension as a function of temperature. Experimental results from the literature and the present work are compared to values obtained from DGT + PC–SAFT as well as predictions by MD simulations. The results from DGT + PC–SAFT are in good agreement with the experimental data from literature [1, 79–82] and from the present work. The MD simulation results show higher values of the interfacial tension as the molecular model for ethanol overestimates the interfacial tension of the pure component by about 25 %.

[Table A.1 about here]

A.3. Saturated densities in the binary mixture of ethanol and CO_2

The results of the PC–SAFT calculations on the density difference $\Delta\rho$ are compared with experimental data as found in the work of Tsivintzelis et al. [19]. Figure A.2 shows the density difference $\Delta\rho$ as a function of pressure. The average

absolute deviation from the experimental data is better than 0.4 % and the maximum absolute deviation does not exceed 0.6 % in the experimental pressure range of the present work.

[Figure A.2 about here]

In addition to experimental data from literature, the liquid densities of pure ethanol and of the binary system ethanol and CO_2 in vapor–liquid equilibrium are also measured at 4 temperatures between 303.1K and 333.1K and pressures up to about 5.5 MPa. The results are listed in Table A.2. The densities of pure ethanol agree well with the model of Dillon and Penoncello [78], as used in REFPROP (version 8.0). The deviation in the density is less than 0.06%.

The experimental results of the saturated liquid density of the binary mixture from the present work are compared to literature data. At 303.1 K, the average absolute deviation from the data of Stievano and Elvassore [14] is less than 1.4 %. At 313.1K, the results agree better than 0.1% with the data of Tsivintzelis et al. [19], better than 0.6% with the data of Chang et al. [83] and better than 0.8% with the data of Stievano and Elvassore [14]. At 323.1K, the average absolute deviation from the data of Stievano and Elvassore amounts 2%. Over the entire temperature range, the average deviation of the PC–SAFT EOS from the experimental liquid density data of this work is better than 0.5%.

[Table A.2 about here]

B. Molecular dynamics simulations

B.1. Simulation details

The molecular simulations were performed with the molecular dynamics code $ls1\ mardyn$ [84, 85] in the canonical ensemble with $N = 16{,}000$ particles. The equation of motion was solved by a leapfrog integrator [86] with a time step of $\Delta t = 1$ fs. The elongation of the simulation volume normal to the interface was 30 nm and the thickness of the liquid film in the center of the simulation volume was 15 nm to account for finite size effects [87]. The elongation in the other spatial directions was at least 6 nm.

Thermodynamic properties in heterogeneous systems are very sensitive to the truncation of the intermolecular potential [57, 88–94]. For the Lennard-Jones potential, a large variety of long-range corrections (LRC) exist for heterogeneous systems to account for the inhomogeneity [95–100]. For polar interactions in most cases methods based on the Ewald summation are used [95–97], which are not favorable for large particle numbers due to the scaling with $\mathcal{O}(N^{3/2})$. For large

systems LRCs based on the density profile are favorable with a linear scaling, i.e. $\mathcal{O}(N)$ [92].

For all of the present simulations, the cutoff radius was set to 17.5 Å and a center-of-mass cutoff scheme was employed. The Lennard-Jones interactions were corrected with a slab-based LRC [99]. Electrostatic interactions were approximated by a resulting effective molecular dipole and corrected with a slab-based LRC [92]. The quadrupolar interactions do not need a LRC as they decay by r^{-10} [101].

The equilibration was executed for 500,000 time steps. The production was conducted for 2,500,000 time steps to reduce statistical uncertainties. The statistical errors were estimated to be three times the standard deviation of five block averages, each over 500,000 time steps. The saturated densities and vapor pressures were calculated as an average over the respective phases excluding the area close to the interface, i.e. the area where the first derivative of the density with respect to the y coordinate deviated from zero significantly.

B.2. Simulation results

The MD simulation results for pure ethanol are given in Table A.3 and for the binary mixtures of ethanol and CO_2 in Table A.4.

[Both Tables A.3 and A.4 about here].

Acknowledgment

The authors gratefully acknowledge financial support by the German Science Foundation within CRC 926 "Microscale Morphology of Component Surfaces". Computational support is acknowledged by the Regional Computing Center Kaiserslautern (RHRK) under the grant TUKL-MSWS. The authors thank Gerd Maurer for helpful discussions and Lukas Übelacker for supporting the experimental work.

[1] J. J. Jasper, The surface tension of pure liquid compounds, J. Phys. Chem. Ref. Data 1 (4) (1972) 841–1010. doi:10.1063/1.3253106.

[2] C. Wohlfarth, B. Wohlfarth, Surface Tension of Pure Liquids and Binary Liquid Mixtures, Vol. 16 of Landolt–Börnstein, Numerical Data and Functional Relationships in Science and Technology, Springer, 1997.

[3] Dortmund data bank, 2015, www.ddbst.com.

[4] B. Eckl, J. Vrabec, H. Hasse, On the application of force fields for predicting a wide variety of properties: Ethylene oxide as an example, Fluid Phase Equilib. 274 (1 - 2) (2008) 16–26. doi:10.1016/j.fluid.2008.02.002.

[5] Y.-L. Huang, T. Merker, M. Heilig, H. Hasse, J. Vrabec, Molecular modeling and simulation of vapor–liquid equilibria of ethylene oxide, ethylene glycol, and water as well as their binary mixtures, Ind. Eng. Chem. Res. 51 (21) (2012) 7428–7440. doi:10.1021/ie300248z.

[6] Y.-L. Huang, M. Heilig, H. Hasse, J. Vrabec, Vapor-liquid equilibria of hydrogen chloride, phosgene, benzene, chlorobenzene, ortho-dichlorobenzene and toluene by molecular simulation, AIChE J. 52 (4) (2011) 1043–1060. doi:10.1002/aic.12329.

[7] S. Werth, K. Stöbener, P. Klein, K.-H. Küfer, M. Horsch, H. Hasse, Molecular modelling and simulation of the surface tension of real quadrupolar fluids, Chemical Engineering Science 121 (2015) 110 – 117. doi:10.1016/j.ces.2014.08.035.

[8] J. Gross, G. Sadowski, Perturbed-Chain SAFT: An equation of state based on a perturbation theory for chain molecules, Ind. Eng. Chem. Res. 40 (4) (2001) 1244–1260. doi:10.1021/ie0003887.

[9] J. Gross, G. Sadowski, Application of the Perturbed-Chain SAFT equation of state to associating systems, Ind. Eng. Chem. Res. 41 (22) (2002) 5510–5515. doi:10.1021/ie010954d.

[10] H. Kahl, S. Enders, Interfacial properties of binary mixtures, Phys. Chem. Chem. Phys. 4 (2002) 931–936. doi:10.1039/B108535M.

[11] S. Enders, H. Kahl, Interfacial properties of water + alcohol mixtures, Fluid Phase Equilibria 263 (2) (2008) 160–167. doi:10.1016/j.fluid.2007.10.006.

[12] A. Kordikowski, A. Schenk, R. V. Nielen, C. Peters, Volume expansions and vapor-liquid equilibria of binary mixtures of a variety of polar solvents and certain near-critical solvents, J. Supercrit. Fluids 8 (3) (1995) 205–216. doi:10.1016/0896-8446(95)90033-0.

[13] B. Seifried, F. Temelli, Density of carbon dioxide expanded ethanol at (313.2, 328.2, and 343.2) K, J. Chem. Eng. Data 55 (7) (2010) 2410–2415. doi:10.1021/je900830s.

[14] M. Stievano, N. Elvassore, High–pressure density and vapor–liquid equilibrium for the binary systems carbon dioxide–ethanol, carbon dioxide–acetone and carbon dioxide–dichloromethane, J. Supercrit. Fluids 33 (1) (2005) 7–14. doi:10.1016/j.supflu.2004.04.003.

[15] H. Tanaka, M. Kato, Vapor–liquid equilibrium properties of carbon dioxide + ethanol mixture at high pressures, J. Chem. Eng. Jpn. 28 (3) (1995) 263–266. doi:10.1252/jcej.28.263.

[16] B. G. Pfohl O., Pagel A., Phase equilibria in systems containing o–cresol, p–cresol, carbon dioxide, and ethanol at 323.15–473.15 K and 10–35 MPa, Fluid Phase Equilib. 157 (1999) 53–79. doi:10.1016/S0378-3812(99)00019-9.

[17] L. Galicia-Luna, A. Ortega-Rodriguez, D. Richon, New apparatus for the fast determination of high-pressure vapor–liquid equilibria of mixtures and of accurate critical pressures, J.Chem.Eng.Data 45 (2) (2000) 265–271. doi:10.1021/je990187d.

[18] C. Secuianu, V. Feroiu, D. Geana, Phase behavior for carbon dioxide + ethanol system: Experimental measurements and modeling with a cubic equation of state, J.Supercrit.Fluids 47 (2) (2008) 109–116. doi:10.1016/j.supflu.2008.08.004.

[19] I. Tsivintzelis, D. Missopolinou, K. Kalogiannis, C. Panayiotou, Phase compositions and saturated densities for the binary systems of carbon dioxide with ethanol and dichloromethane, Fluid Phase Equilib. 224 (1) (2004) 89–96. doi:10.1016/j.fluid.2004.06.046.

[20] Y. Sun, B. Y. Shekunov, Surface tension of ethanol in supercritical CO_2, J. Supercrit. Fluids 27 (1) (2003) 73–83. doi:10.1016/S0896-8446(02)00184-5.

[21] D. Dittmar, A. Fredenhagen, S. Oei, R. Eggers, Interfacial tensions of ethanol–carbon dioxide and ethanol–nitrogen. dependence of the interfacial tension on the fluid density – prerequisites and physical reasoning, Chem. Eng. Sci. 58 (7) (2003) 1223–1233. doi:10.1016/S0009-2509(02)00626-7.

[22] D. Dittmar, Untersuchungen zum Stofftransport über Fluid/Flüssig Phasengrenzen in Systemen unter erhöhten Drücken, Dissertation, Institut für Thermische Verfahrenstechnik, Hamburg; Shaker, Aachen, 2008.

[23] J. W. Gibbs, The Scientific Papers of J. W. Gibbs, Dover Publications, 1961.

[24] H. Kahl, T. Wadewitz, J. Winkelmann, Surface tension of pure liquids and binary liquid mixtures, J. Chem. Eng. Data 48 (3) (2003) 580–586. doi:10.1021/je0201323.

[25] H. Kahl, T. Wadewitz, J. Winkelmann, Surface tension and interfacial tension of binary organic liquid mixtures, J. Chem. Eng. Data 48 (6) (2003) 1500–1507. doi:10.1021/je034062r.

[26] H. Renon, J. M. Prausnitz, Local compositions in thermodynamic excess functions for liquid mixtures, AIChE J. 14 (1) (1968) 135–144. doi:10.1002/aic.690140124.

[27] W. L. Masterton, J. Bianchi, E. J. Slowinski, Surface tension and adsorption in gas–liquid systems at moderate pressures, J. Phys. Chem. 67 (3) (1963) 615–618. doi:10.1021/j100797a018.

[28] A. Mejía, M. Cartes, H. Segura, E. A. Müller, Use of equations of state and coarse grained simulations to complement experiments: Describing the interfacial properties of carbon dioxide + decane and carbon dioxide + eicosane mixtures, J. Chem. Eng. Data 59 (10) (2014) 2928–2941. doi:10.1021/je5000764.

[29] D. J. Lee, M. M. Telo da Gama, K. E. Gubbins, Adsorption and surface tension reduction at the vapor-liquid interface, J. Phys. Chem. 89 (8) (1985) 1514–1519. doi:10.1021/j100254a041.

[30] E. A. Müller, A. Mejía, Resolving discrepancies in the measurements of the interfacial tension for the CO_2 + H_2O mixture by computer simulation, J. Phys. Chem. Lett. 5 (7) (2014) 1267–1271. doi:10.1021/jz500417w.

[31] J. M. Garrido, L. Cifuentes, M. Cartes, H. Segura, A. Mejía, High-pressure interfacial tensions for nitrogen + ethanol, or hexane or 2-methoxy-2-methylbutane: A comparison between experimental tensiometry and Monte Carlo simulations, J. Supercrit. Fluids 89 (2014) 78–88. doi:10.1016/j.supflu.2014.02.012.

[32] B. S. Carey, L. E. Scriven, H. T. Davis, Semiempirical theory of surface tension of binary systems, AIChE J. 26 (5) (1980) 705–711. doi:10.1002/aic.690260502.

[33] P. Cornelisse, C. Peters, J. de Swaan Arons, Non-classical interfacial tension and fluid phase behaviour, Fluid Phase Equilib. 117 (1–2) (1996) 312–319. doi:10.1016/0378-3812(95)02968-0.

[34] Y.-X. Zuo, E. H. Stenby, Calculation of interfacial tensions with gradient theory, Fluid Phase Equilib. 132 (1 – 2) (1997) 139–158. doi:10.1016/S0378-3812(96)03152-4.

[35] P. Cornelisse, M. Wijtkamp, C. Peters, J. de Swaan Arons, Interfacial tensions of fluid mixtures with polar and associating components, Fluid Phase Equilib. 150 - 151 (1998) 633–640. doi:10.1016/S0378-3812(98)00311-2.

[36] H. Kahl, S. Enders, Calculation of surface properties of pure fluids using density gradient theory and SAFT-EOS, Fluid Phase Equilib. 172 (1) (2000) 27–42. doi:10.1016/S0378-3812(00)00361-7.

[37] C. Miqueu, B. Mendiboure, C. Graciaa, J. Lachaise, Modelling of the surface tension of binary and ternary mixtures with the gradient theory of fluid interfaces, Fluid Phase Equilib. 218 (2) (2004) 189–203. doi:10.1016/j.fluid.2003.12.008.

[38] S. Enders, H. Kahl, J. Winkelmann, Surface tension of the ternary system water + acetone + toluene, J. Chem. Eng. Data 52 (3) (2007) 1072–1079. doi:10.1021/je7000182.

[39] C. Cumicheo, M. Cartes, H. Segura, E. A. Müller, A. Mejía, High-pressure densities and interfacial tensions of binary systems containing carbon dioxide + n-alkanes: (n-dodecane, n-tridecane, n-tetradecane), Fluid Phase Equilibria 380 (2014) 82–92. doi:10.1016/j.fluid.2014.07.039.

[40] T. Lafitte, B. Mendiboure, M. M. Piñeiro, D. Bessières, C. Miqueu, Interfacial properties of water/CO_2: A comprehensive description through a gradient theory – SAFT–VR Mie approach, J. Phys. Chem. B 114 (34) (2010) 11110–11116. doi:10.1021/jp103292e.

[41] X.-S. Li, J.-M. Liu, D. Fu, Investigation of interfacial tensions for carbon dioxide aqueous solutions by perturbed-chain statistical associating fluid theory combined with density-gradient theory, Ind. Eng. Chem. Res. 47 (22) (2008) 8911–8917. doi:10.1021/ie800959h.

[42] G. Niño-Amézquita, D. van Putten, S. Enders, Phase equilibrium and interfacial properties of water + CO_2 mixtures, Fluid Phase Equilib. 332 (2012) 40–47. doi:10.1016/j.fluid.2012.06.018.

[43] E. Schäfer, G. Sadowski, S. Enders, Interfacial tension of binary mixtures exhibiting azeotropic behavior: Measurement and modeling with PCP-SAFT combined with density gradient theory, Fluid Phase Equilib. 362 (2014) 151–162. doi:10.1016/j.fluid.2013.09.042.

[44] C. I. Poser, I. C. Sanchez, Interfacial tension theory of low and high molecular weight liquid mixtures, Macromolecules 14 (2) (1981) 361–370. doi:10.1021/ma50003a026.

[45] S. Hartland, R. Hartley, Axisymmetric Fluid–Liquid Interfaces, Elsevier, Amsterdam, 1976.

[46] B. Song, J. Springer, Determination of interfacial tension from the profile of a pendant drop using computer-aided image processing: 1. theoretical, J. Colloid Interface Sci. 184 (1) (1996) 64–76. doi:10.1006/jcis.1996.0597.

[47] T. Wadewitz, J. Winkelmann, Density functional theory: structure and interfacial properties of binary mixtures, Ber. Bunsenges. Phys. Chem. 100 (11) (1996) 1825–1832. doi:10.1002/bbpc.19961001112.

[48] T. Merker, C. Engin, J. Vrabec, H. Hasse, Molecular model for carbon dioxide optimized to vapor–liquid equilibria, The Journal of Chemical Physics 132 (23) (2010) 234512. doi:10.1063/1.3434530.

[49] T. Schnabel, J. Vrabec, H. Hasse, Henry's law constants of methane, nitrogen, oxygen and carbon dioxide in ethanol from 273 to 498 K: Prediction from molecular simulation, Fluid Phase Equilib. 233 (2005) 134–143. doi:10.1016/j.fluid.2005.04.016.

[50] S. Reiser, N. McCann, M. Horsch, H. Hasse, Hydrogen bonding of ethanol in supercritical mixtures with CO_2 by ^{1}H NMR spectroscopy and molecular simulation, J. Supercrit. Fluids 68 (2012) 94–103. doi:10.1016/j.supflu.2012.04.014.

[51] K. Langenbach, C. Engin, S. Reiser, M. Horsch, H. Hasse, On the simultaneous description of h–bonding and dipolar interactions with point charges in force field models, AIChE J. 61 (9) (2015) 2926–2932. doi:10.1002/aic.14820.

[52] C. G. Gray, K. E. Gubbins, Theory of Molecular Fluids, Vol. 1: Fundamentals, Clarendon Press, Oxford, 1984.

[53] H. A. Lorentz, Ueber die anwendung des satzes vom virial in der kinetischen theorie der gase, Ann. Phys. 12 (1881) 127–136. doi:10.1002/andp.18812480110.

[54] D. Berthelot, Sur le mélange des gaz, Compt. Rend. Ac. Sc. 126 (1898) 1703–1706.

[55] T. Schnabel, J. Vrabec, H. Hasse, Unlike lennard–jones parameters for vapor–liquid equilibria, J. Mol. Liq. 135 (2007) 170–178. doi:10.1016/j.molliq.2006.12.024.

[56] C. Caleman, P. J. van Maaren, M. Hong, J. S. Hub, L. T. Costa, D. van der Spoel, Force field benchmark of organic liquids: Density, enthalpy of vaporization, heat capacities, surface tension, isothermal compressibility, volumetric expansion coefficient, and dielectric constant, J. Chem. Theory Comput. 8 (1) (2012) 61–74. doi:10.1021/ct200731v.

[57] R. A. Zubillaga, A. Labastida, B. Cruz, J. C. Martinez, E. Sanchez, J. Alejandre, Surface tension of organic liquids using the OPLS/AA force field, J. Chem. Theory Comput. 9 (3) (2013) 1611–1615. doi:10.1021/ct300976t.

[58] S. Eckelsbach, J. Vrabec, Fluid phase interface properties of acetone, oxygen, nitrogen and their binary mixtures by molecular simulation, Phys. Chem. Chem. Phys. 17 (40) (2015) 27195–27203. doi:10.1039/C5CP03415A.

[59] J.-C. Neyt, A. Wender, V. Lachet, P. Malfreyt, Modeling the pressure dependence of acid gas + n-alkane interfacial tensions using atomistic

Monte Carlo simulations, J. Phys. Chem. C 116 (19) (2012) 10563–10572. doi:10.1021/jp212004c.

[60] C. Avendaño, T. Lafitte, A. Galindo, C. Adjiman, G. Jackson, E. Müller, Saft–γ force field for the simulation of molecular fluids. 1. a single-site coarse grained model of carbon dioxide, J. Phys. Chem. B 115 (38) (2011) 11154–11169. doi:10.1021/jp204908d.

[61] C. Avendaño, T. Lafitte, C. Adjiman, A. Galindo, E. Müller, G. Jackson, Saft–γ force field for the simulation of molecular fluids: 2. coarse-grained models of greenhouse gases, refrigerants, and long alkanes, J. Phys. Chem. B 117 (9) (2013) 2717–2733. doi:10.1021/jp306442b.

[62] C. Herdes, T. S. Totton, E. A. Müller, Coarse grained force field for the molecular simulation of natural gases and condensates, Fluid Phase Equilib. 406 (2015) 91–100. doi:10.1016/j.fluid.2015.07.014.

[63] N. Ferrando, V. Lachet, J. Pérez-Pellitero, A. D. Mackie, P. Malfreyt, A transferable force field to predict phase equilibria and surface tension of ethers and glycol ethers, J. Phys. Chem. B 115 (36) (2011) 10654–10664. doi:10.1021/jp203278t.

[64] S. K. Singh, A. Sinha, G. Deo, J. K. Singh, Vapor–liquid phase coexistence, critical properties, and surface tension of confined alkanes, J. Phys. Chem. C 113 (17) (2009) 7170–7180. doi:10.1021/jp8073915.

[65] S. Eckelsbach, S. Miroshnichenko, G. Rutkai, J. Vrabec, Surface tension, large scale thermodynamic data generation and vapor–liquid equilibria of real compounds, in: W. E. Nagel, D. B. Kröner, M. M. Resch (Eds.), High Performance Computing in Science and Engineering '13, Springer, Berlin/Heidelberg, 2013, pp. 635–646.

[66] J.-C. Neyt, A. Wender, V. Lachet, P. Malfreyt, Prediction of the temperature dependence of the surface tension of SO_2, N_2, O_2, and Ar by Monte Carlo molecular simulations, J. Phys. Chem. B 115 (30) (2011) 9421–9430. doi:10.1021/jp204056d.

[67] S. Werth, K. Stöbener, P. Klein, K.-H. Küfer, M. Horsch, H. Hasse, Molecular modelling and simulation of the surface tension of real quadrupolar fluids, Chem. Eng. Sci. 121 (2015) 110–117. doi:10.1016/j.ces.2014.08.035.

[68] S. Werth, M. Horsch, H. Hasse, Surface tension of the two center lennard–jones plus point dipole fluid, J. Chem. Phys. 144 (2016) 054702. doi:10.1063/1.4940966.

[69] J. P. R. B. Walton, D.-J. Tildesley, J. S. Rowlinson, J. R. Henderson, The pressure tensor at the planar surface of a liquid, Mol. Phys. 48 (6) (1983) 1357–1368. doi:10.1080/00268978300100971.

[70] J. G. Kirkwood, F. P. Buff, The statistical mechanical theory of surface tension, J. Chem. Phys. 17 (3) (1949) 338–343. doi:10.1063/1.1747248.

[71] J. D. van der Waals, Over de Continuiteit van den Gas- en Vloeistoftoestand, Ph.D. thesis, Universiteit Leiden (1873).

[72] J. W. Cahn, J. E. Hilliard, Free energy of a nonuniform system. i. interfacial free energy, J. Chem. Phys. 28 (2) (1958) 258–267. doi:10.1063/1.1744102.

[73] C. Miqueu, B. Mendiboure, A. Garciaa, J. Lachaise, Modeling of the surface tension of multicomponent mixtures with the gradient theory of fluid interfaces, Ind. Eng. Chem. Res. 44 (9) (2005) 3321–3329. doi:10.1021/ie049086l.

[74] S. Enders, H. Kahl, J. Winkelmann, Interfacial properties of polystyrene in contact with carbon dioxide, Fluid Phase Equilib. 228 - 229 (2005) 511–522. doi:10.1016/j.fluid.2004.10.001.

[75] K. Langenbach, S. Enders, Cross–association of multi–component systems, Mol. Phys. 110 (2012) 1249–1260. doi:10.1080/00268976.2012.668963.

[76] M. Kleiner, , G. Sadowski, Modeling of polar systems using PCP-SAFT: An approach to account for induced-association interactions, J. Phys. Chem. C 111 (43) (2007) 15544–15553. doi:10.1021/jp072640v.

[77] J. Gross, An equation of state contribution for polar components: Quadrupolar molecules, AIChE J. 51 (9) (2005) 2556–2568. doi:10.1002/aic.10502.
URL

[78] H. Dillon, S. Penoncello, A fundamental equation for calculation of the thermodynamic properties of ethanol, Int. J. Thermophys. 25 (2) (2004) 321–335. doi:10.1023/B:IJOT.0000028470.49774.14.

[79] G. N. Muratov, Surface tension of benzene and ethanol, Zh. Fiz. Khim. 54 (8) (1980) 2088–2089.

[80] Y. V. Efremov, Desnsity, surface tension, vapor pressure, and critical parameters of alcohols, Zh. Fiz. Khim. 40 (6) (1966) 667–671.

[81] G. Vazquez, E. Alvarez, J. M. Navaza, Surface tension of alcohol water + water from 20 to 50 °C, J. Chem. Eng. Data 40 (3) (1995) 611–614. doi:10.1021/je00019a016.

[82] E. Álvarez, A. Correa, J. M. Correa, E. García-Rosello, J. M. Navaza, Surface tensions of three amyl alcohol + ethanol binary mixtures from (293.15 to 323.15) K, J. Chem. Eng. Data 56 (11) (2011) 4235–4238. doi:10.1021/je200793z.

[83] C. J. Chang, C.-Y. Day, C.-M. Ko, K.-L. Chiu, Densities and p-x-y diagrams for carbon dioxide dissolution in methanol, ethanol, and acetone mixtures, Fluid Phase Equilib. 131 (1–2) (1997) 243–258. doi:10.1016/S0378-3812(96)03208-6.

[84] C. Niethammer, S. Becker, M. Bernreuther, M. Buchholz, W. Eckhardt, A. Heinecke, S. Werth, H.-J. Bungartz, C. W. Glass, H. Hasse, J. Vrabec, M. Horsch, *ls1 mardyn*: The massively parallel molecular dynamics code for large systems, J. Chem. Theory Comput. 10 (10) (2014) 4455–4464. doi:10.1021/ct500169q.

[85] W. Eckhardt, A. Heinecke, R. Bader, M. Brehm, N. Hammer, H. Huber, H.-G. Kleinhenz, J. Vrabec, H. Hasse, M. Horsch, M. Bernreuther, C. W. Glass, C. Niethammer, A. Bode, H.-J. Bungartz, Supercomputing - XXVIII. International Supercomputing Conference (ISC 2013), Vol. 7905 of LNCS, Springer, Heidelberg, 2013, Ch. 1, pp. 1–12.

[86] D. Fincham, Leapfrog rotational algorithms, Mol. Sim. 8 (3-5) (1992) 165–178. doi:10.1080/08927029208022474.

[87] S. Werth, S. V. Lishchuk, M. Horsch, H. Hasse, The influence of the liquid slab thickness on the planar vapor–liquid interfacial tension, Physica A 392 (10) (2013) 2359–2367. doi:10.1016/j.physa.2013.01.048.

[88] F. Goujon, P. Malfreyt, D.-J. Tildesley, The gas–liquid surface tension of argon: A reconciliation between experiment and simulation, J. Chem. Phys. 140 (2014) 244710. doi:10.1063/1.4885351.

[89] S. Werth, M. Horsch, J. Vrabec, H. Hasse, Comment on "the gas–liquid surface tension of argon: A reconciliation between experiment and simulation" [j. chem. phys. 140, 244710 (2014)], J. Chem. Phys. 142 (2015) 107101. doi:10.1063/1.4914149.

[90] F. Goujon, P. Malfreyt, D.-J. Tildesley, Response to "comment on 'the gas-liquid surface tension of argon: A reconciliation between experiment and simulation"' [j. chem. phys. 142, 107101 (2015)], J. Chem. Phys. 142 (2015) 107102. doi:10.1063/1.4914150.

[91] F. Goujon, A. Ghoufi, P. Malfreyt, D.-J. Tildesley, Controlling the long-range corrections in atomistic Monte Carlo simulations of two–phase systems, J. Chem. Theory Comput. 11 (10) (2015) 4573–4585. doi:10.1021/acs.jctc.5b00377.

[92] S. Werth, M. Horsch, H. Hasse, Long–range correction for dipolar fluids at planar interfaces, Mol. Phys. 113 (23) (2015) 3750–3756. doi:10.1080/00268976.2015.1061151.

[93] G. Galliero, M. M. Piñeiro, B. Mendiboure, C. Miqueu, T. Lafitte, D. Bessieres, Interfacial properties of the mie n–6 fluid: Molecular simulations and gradient theory results, J. Chem. Phys. 130 (2009) 104704. doi:10.1063/1.3085716.

[94] O. Lobanova, C. Avendaño, T. Lafitte, E. A. Müller, G. Jackson, Saft–γ force field for the simulation of molecular fluids: 4. a single–site coarse–grained model of water applicable over a wide temperature range, Mol. Phys. 113 (9-10) (2015) 1228–1249. doi:10.1080/00268976.2015.1004804.

[95] P. J. in 't Veld, A. E. Ismail, G. S. Grest, Application of ewald summations to long–range dispersion forces, J. Chem. Phys. 127 (2007) 144711. doi:10.1063/1.2770730.

[96] R. E. Isele-Holder, W. Mitchell, A. E. Ismail, Development and application of a particle-particle particle-mesh ewald method for dispersion interactions, J. Chem. Phys. 137 (2012) 174107. doi:10.1063/1.4764089.

[97] R. E. Isele-Holder, W. Mitchell, J. R. Hammond, A. Kohlmeyer, A. E. Ismail, Reconsidering dispersion potentials: Reduced cutoffs in mesh-based ewald solvers can be faster than truncation, J. Chem. Theory Comput. 9 (12) (2013) 5412. doi:10.1021/ct4004614.

[98] D. Tameling, P. Springer, P. Bientinesi, A. E. Ismail, Multilevel summation for dispersion: A linear-time algorithm for r^{-6} potentials, J. Chem. Phys. 140 (2014) 024105. doi:10.1063/1.4857735.

[99] S. Werth, G. Rutkai, J. Vrabec, M. Horsch, H. Hasse, Long range correction for multi–site lennard–jones models and planar interfaces, Mol. Phys. 112 (17) (2014) 2227–2234. doi:10.1080/00268976.2013.861086.

[100] J. Janeček, Long range corrections in inhomogeneous simulations, J. Phys. Chem. B 110 (12) (2006) 6264–6269. doi:10.1021/jp056344z.

[101] J. M. Prausnitz, R. N. Lichtenthaler, E. G. de Azevedo, Molecular Thermodynamics of Fluid-Phase Equilibria, Pearson Education, New Jersey, 1998.

Figures

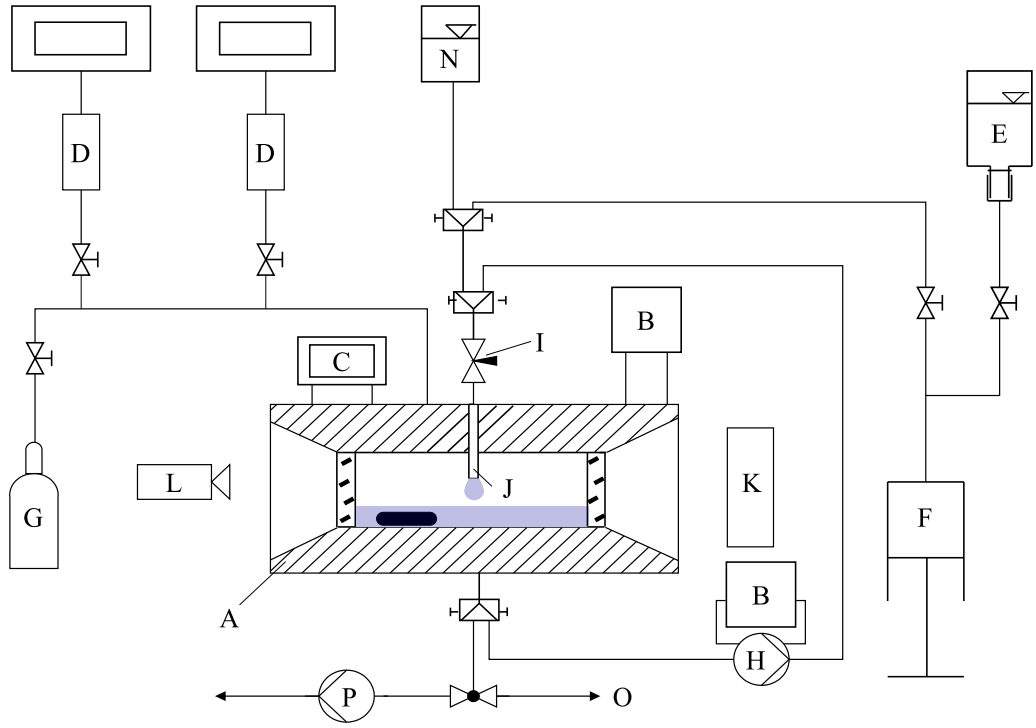

Figure 1: Apparatus for the measurement of interfacial tensions of pure fluids and fluid mixtures at elevated pressures. A: cylindrical high pressure view cell with sapphire windows and magnetic stirrer; B: thermostat; C: platinum resistance thermometer; D: pressure gauge; E: pure solvent; F: hand pump; G: gas container; H: dosing pump; I: needle valve; J: capillary; K: diffuse LED luminous field; L: CCD–camera with objective lens; N: tank for rinsing solvent; O: solvent outlet; P: vacuum pump with cooling trap.

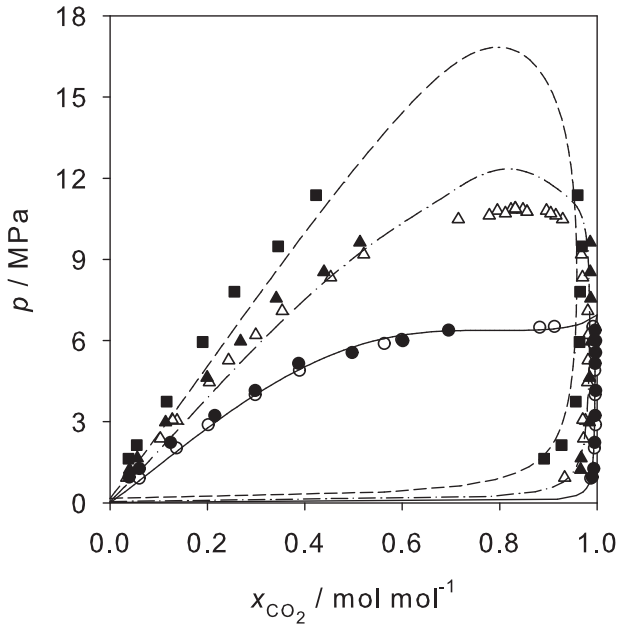

Figure 2: Vapor–liquid equilibrium of the binary system ethanol + CO_2 at temperatures of: 303.2 K (○, Secuianu et al. [18]; ●, MD simulation; ———, PC–SAFT EOS), about 333.5 K (△, Galicia–Luna et al. [17]; ▲, MD simulation; —·— , PC–SAFT EOS), and 363.2 K (■, MD simulation; — — — , PC–SAFT EOS).

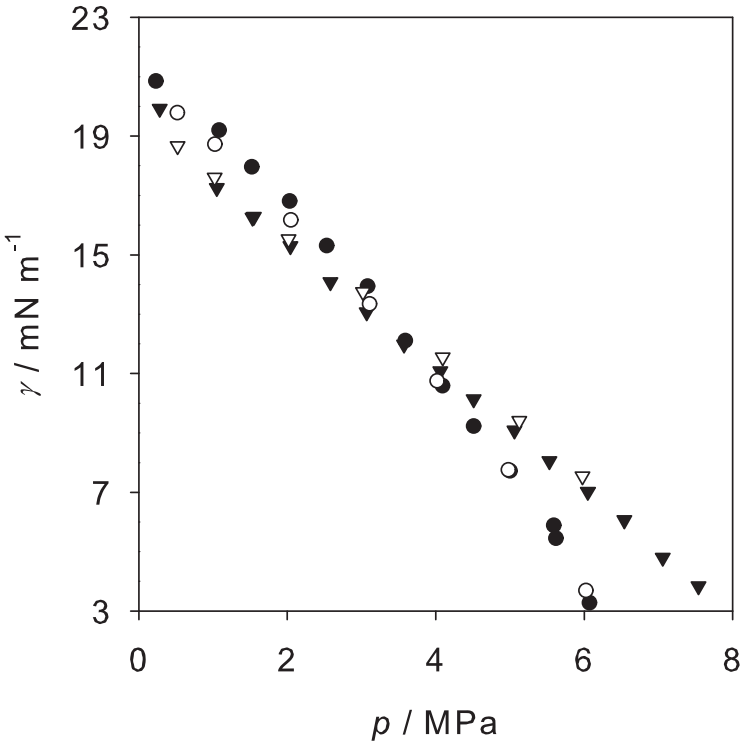

Figure 3: Experimental data for the interfacial tension in the binary system ethanol + CO_2 as a function of pressure. This work: ○, 303.2 K; ▽, 323.2 K. Dittmar [22]: ●, 303.5 K; ▼, 323.7 K.

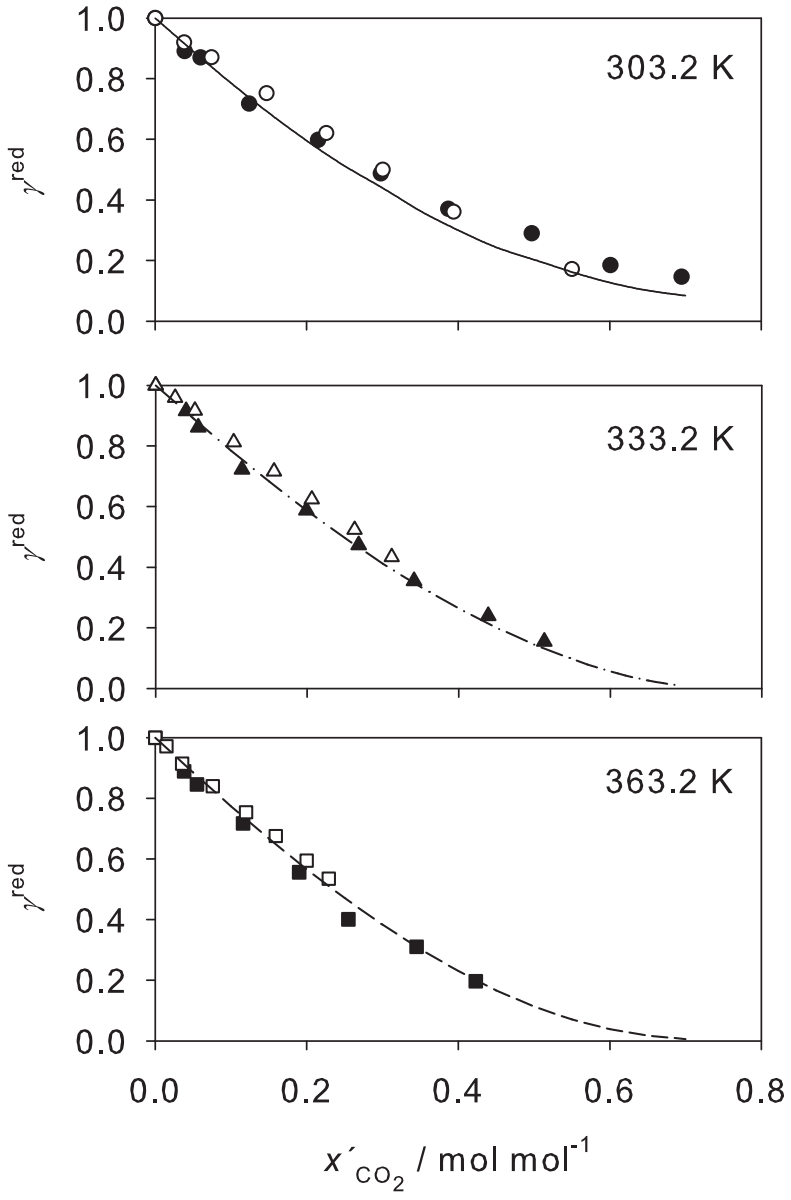

Figure 4: Isotherms of the reduced interfacial tension γ^{red}, see Eq. (17), as a function of the mole fraction of CO_2 in the liquid phase at temperatures of: 303.2 K (○, experimental; ●, molecular simulation; ———, DGT+PC–SAFT), 333.2 K (△, experimental; ▲, molecular simulation; —·— , DGT+PC–SAFT), 363.2 K (□, experimental; ■, molecular simulation; – – – , DGT+PC–SAFT).

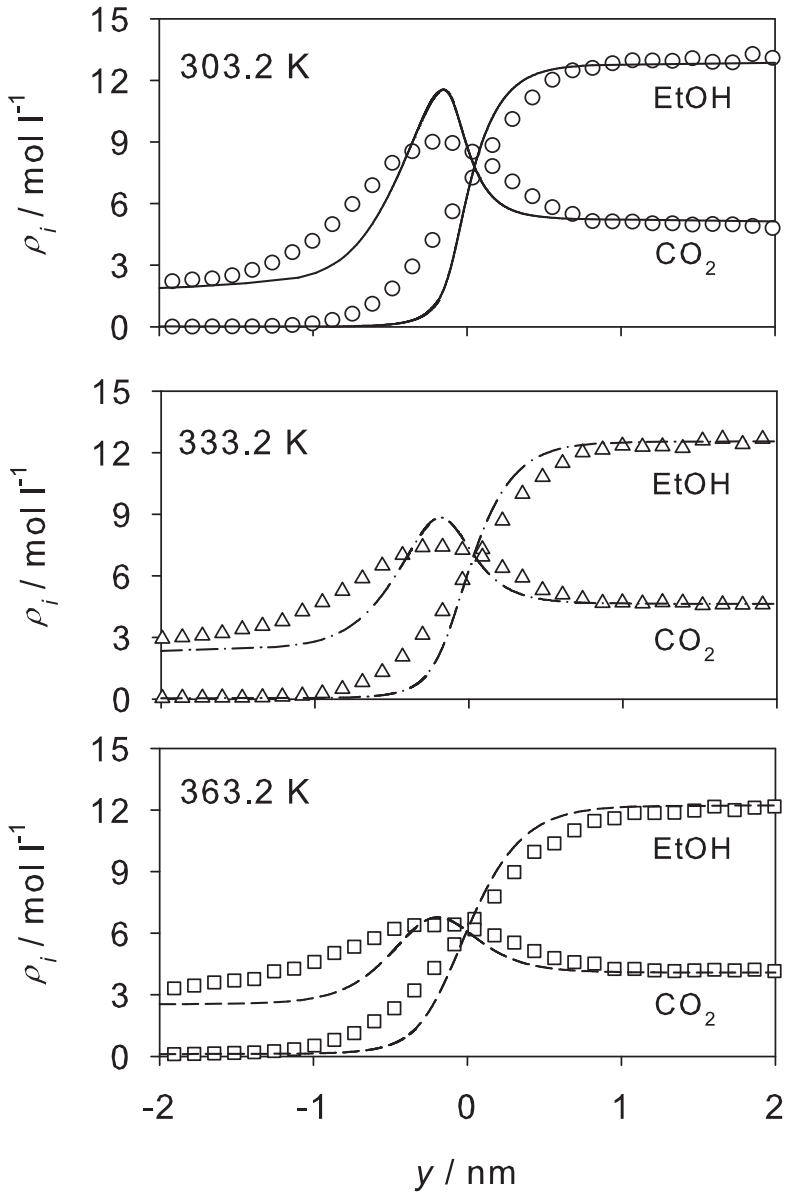

Figure 5: Component density profiles of ethanol and CO_2 at the interface at 303.2 K and x'_{CO_2} = 0.29 mol/mol (top), 333.2 K and x'_{CO_2} = 0.27 mol/mol (middle), as well as 363.2 K and x'_{CO_2} = 0.25 mol/mol (bottom). Symbols: MD simulation; lines: DGT + PC–SAFT.

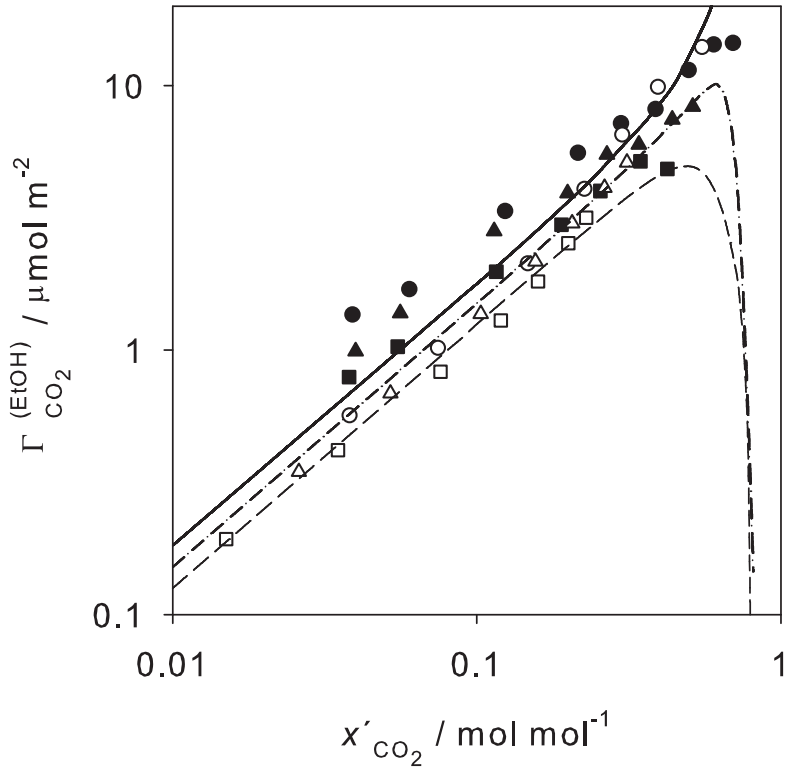

Figure 6: Isotherms of the adsorption of CO_2 relative to ethanol at the interface versus the mole fraction of CO_2 in the liquid phase at temperatures of 303.2 K (○, experimental; ●, MD simulation; ———, DGT+PC–SAFT), 333.2 K (△, experimental; ▲, MD simulation; —·—, DGT+PC–SAFT), 363.2 K (□, experimental; ■, MD simulation; – – –, DGT+PC–SAFT).

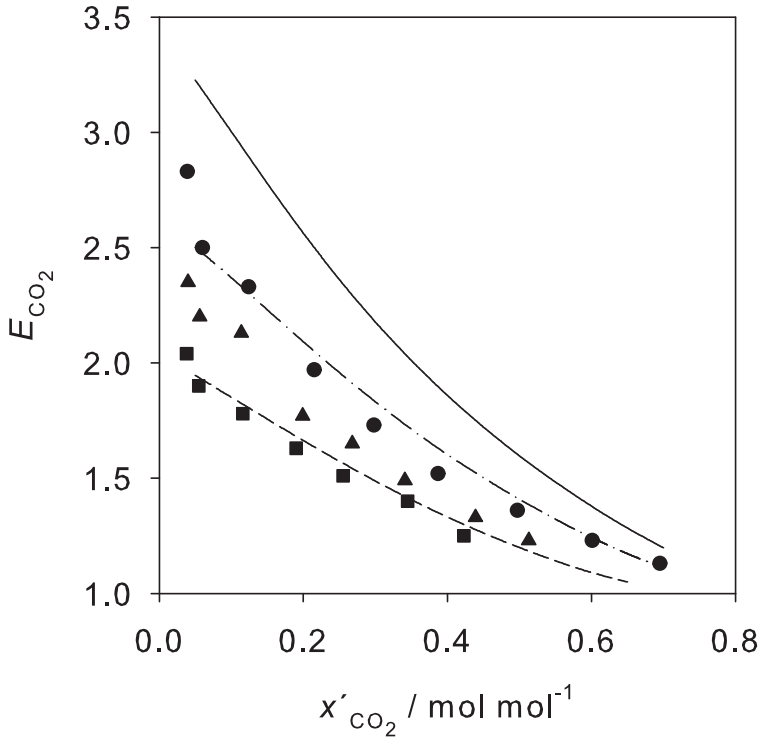

Figure 7: Isotherms of the enrichment of CO_2 versus the mole fraction of CO_2 in the liquid phase at temperatures of: 303.2 K (●, MD simulation; ———, DGT+PC–SAFT), 333.2 K (▲, MD simulation; —·— , DGT+PC–SAFT), 363.2 K (■, MD simulation; – – – , DGT+PC–SAFT).

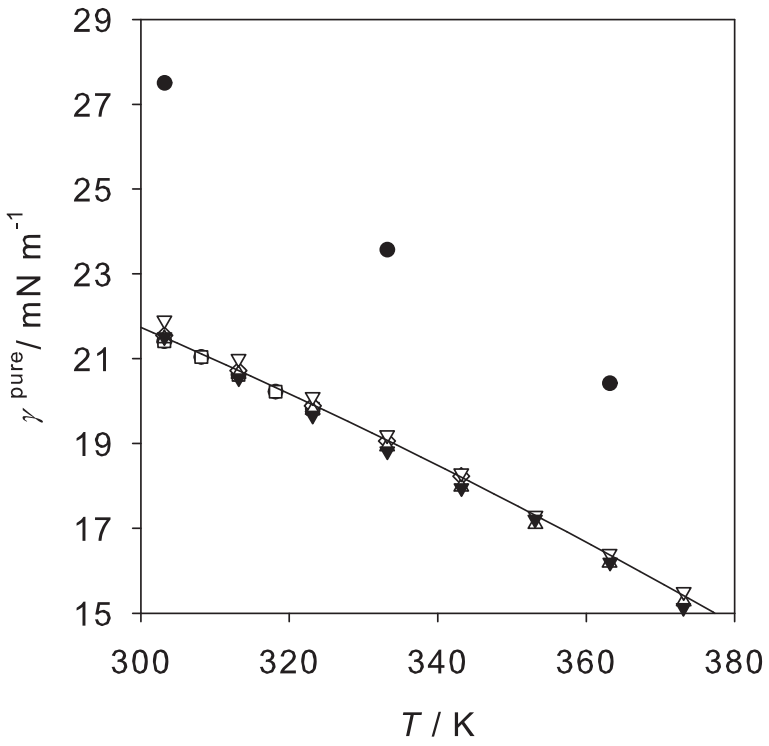

Figure A.1: Interfacial tension of pure ethanol: Comparison of the present experimental and simulation results with experimental data from literature[1, 79–82]. Experimental data: ▼, this work; ◇, Jasper [1]; △, Muratov [79]; ▽, Efremov [80]. ⊕, Vazquez et al. [81]; □, Álvarez et al. [82]; MD simulations from this work: ●. The solid line is the present DGT + PC–SAFT result.

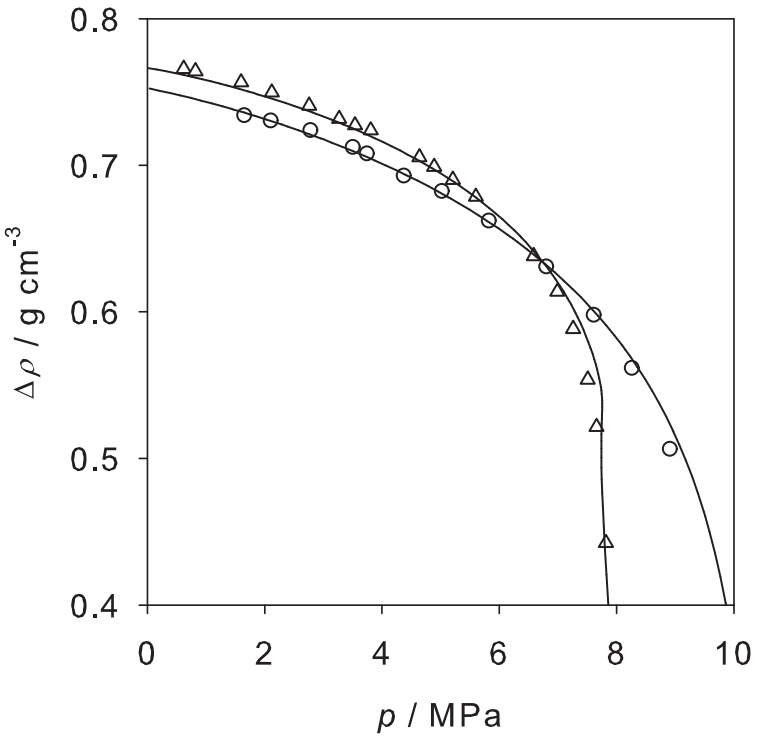

Figure A.2: Difference between the saturated liquid phase density and the saturated vapor phase density $\Delta\rho$ in the binary system ethanol + CO_2. Experimental results by Tsivintzelis et al. [19] at temperatures of 313.2 K (○) and 328.2 K (△). The lines represent the present calculations with the PC–SAFT EOS at the corresponding temperatures.

Tables

Table 1: Description of the chemicals used in the present work.

Chemical name	CAS Number	Supplier	Purity (mole fraction)
carbon dioxide	124-38-9	Air Liquide, France	> 0.99995
ethanol	64-17-5	Merck KGaA, Germany	> 0.999

Table 2: Pure component PC-SAFT and DGT parameters.

compound	m	σ	ε/k_B	$10^4\kappa^{AB}$	$\varepsilon^{AB}/k_\mathrm{B}$	n_P	n_E	Ref.
-	1	Å	K	1	K	1	1	-
CO_2	2.0729	2.7852	169.21	-	-	0	4	[8, 76]
Ethanol	2.3827	3.1771	198.24	0.032384	2653.4	1	1	[9]

Table 3: Interfacial tension γ of the binary mixture ethanol + CO_2 (experimental data of this work).[a]

T / K	p / MPa	γ / mN m^{-1}	T / K	p / MPa	γ / mN m^{-1}
303.2	0.518	19.78	343.2	0.572	16.98
	1.024	18.73		1.079	16.23
	2.046	16.17		2.049	14.68
	3.107	13.35		3.026	13.11
	4.019	10.75		4.122	11.43
	4.979	7.76		5.067	9.93
	6.022	3.69		6.049	8.33
313.2	0.517	19.43	353.2	0.500	16.30
	1.053	18.42		1.009	15.63
	2.024	15.91		2.049	14.15
	3.041	14.11		2.997	12.75
	4.027	11.33		3.999	11.32
	5.105	8.71		5.052	9.85
	6.036	6.23		6.128	8.29
323.2	0.521	18.66	363.2	0.509	15.74
	1.019	17.60		0.994	14.82
	2.019	15.52		1.973	13.61
	3.020	13.75		3.043	12.22
	4.094	11.54		4.024	10.94
	5.125	9.40		5.047	9.63
	5.976	7.54		5.775	8.67
333.2	0.515	18.05	373.1	0.514	14.61
	1.005	17.25		1.025	13.90
	1.993	15.29		2.050	12.84
	3.029	13.47		2.983	11.69
	3.996	11.74		4.051	10.41
	5.078	9.85		5.170	9.05
	5.984	8.16		5.818	8.35

[a] Standard uncertainties u are $u(T) = 0.1$ K, $u(p) = 0.0025$ MPa for $p \leq 2.5$ MPa, and $u(p) = 0.01$ MPa for $p > 2.5$ MPa. The expanded combined uncertainty in the interfacial tension is $U_c(\gamma) = 0.019\,\gamma$.

Table A.1: Interfacial tension γ^{pure} of pure ethanol (experimental data of this work).[a]

T / K	γ^{pure} / mN m^{-1}
303.2	21.51
313.2	20.54
323.1	19.66
333.2	18.82
343.2	17.95
353.1	17.21
363.2	16.20
373.1	15.13

[a] The standard uncertainty u is $u(T)$ = 0.1 K and the expanded uncertainty $U_c(\gamma^{\text{pure}}) = 0.015\ \gamma^{\text{pure}}$.

Table A.2: Saturated liquid densities of pure ethanol and of the binary system ethanol + CO_2 (experimental data of this work). At each temperature, the density at the lowest pressure corresponds to pure ethanol.[a]

T / K	p / MPa	ρ' / g cm^{-3}	T / K	p / MPa	ρ' / g cm^{-3}
303.1	0.014	0.781	323.1	0.059	0.763
	1.121	0.789		1.027	0.770
	2.130	0.800		2.119	0.778
	3.993	0.826		3.373	0.786
	4.688	0.834		4.108	0.791
				4.997	0.797
313.1	0.038	0.772	333.1	0.085	0.754
	1.135	0.780		1.142	0.759
	2.016	0.787		1.974	0.763
	2.877	0.795		2.860	0.766
	3.958	0.803		3.714	0.767
	4.977	0.811		4.737	0.769
	5.274	0.813		5.523	0.771

[a] Standard uncertainties u are $u(T) = 0.1$ K, $u(p) = 0.0025$ MPa for $p \leq 2.5$ MPa, and $u(p) = 0.01$ MPa for $p > 2.5$ MPa. The expanded combined uncertainty in the saturated liquid densities of the binary mixture is $U_c(\rho') = 0.003\ \rho'$.

Table A.3: Molecular simulation results of the vapor-liquid equilibrium of pure ethanol. The number in parentheses indicates the statistical uncertainty in the last decimal digit.

T / K	p / MPa	ρ' / g cm^{-3}	ρ'' / g cm^{-3}	γ / mN m^{-1}
303.2	0.008(1)	0.7867(25)	0.0002(1)	27.5(21)
333.2	0.039(14)	0.7585(30)	0.0007(1)	23.6(20)
363.2	0.133(22)	0.7242(14)	0.0024(6)	20.4(9)

Table A.4: Molecular dynamics simulation results of the vapor-liquid equilibrium of mixtures containing Ethanol and CO_2. The number in parentheses indicates the statistical uncertainty in the last decimal digit.

T / K	p / MPa	ρ' / g cm^{-3}	ρ'' / g cm^{-3}	x'_{CO_2} / mol mol^{-1}	x''_{CO_2} / mol mol^{-1}	γ / mN m^{-1}	Γ / μmol m^{-2}	E_{CO_2}
303.2	0.92(10)	0.7908(12)	0.0175(21)	0.042(7)	0.991(5)	24.5(15)	1.3(3)	2.8(7)
	1.21(12)	0.7936(11)	0.0224(22)	0.064(8)	0.993(6)	24.1(23)	1.5(3)	2.5(7)
	2.23(10)	0.8007(22)	0.0440(9)	0.123(8)	0.995(4)	19.7(22)	3.4(5)	2.33(34)
	3.23(31)	0.8126(35)	0.068(8)	0.215(7)	0.996(4)	16.4(21)	5.6(8)	1.97(16)
	4.15(35)	0.8177(26)	0.093(5)	0.298(8)	0.997(3)	13.4(21)	7.2(7)	1.73(10)
	5.18(25)	0.8263(41)	0.126(9)	0.386(8)	0.995(2)	10.2(16)	8.6(12)	1.52(8)
	5.57(29)	0.834(5)	0.144(13)	0.497(13)	0.997(3)	8.0(16)	11.5(24)	1.36(11)
	6.02(39)	0.836(13)	0.169(29)	0.599(33)	0.998(2)	4.9(17)	14.6(34)	1.23(7)
	6.38(46)	0.829(9)	0.199(35)	0.695(35)	0.996(3)	4.0(14)	15(5)	1.13(10)
333.2	1.19(8)	0.7607(17)	0.0205(25)	0.042(6)	0.965(12)	21.6(28)	0.9(3)	2.3(8)
	1.62(6)	0.7604(26)	0.0280(12)	0.059(3)	0.966(15)	20.5(22)	1.3(1)	2.20(14)
	2.98(17)	0.7693(3)	0.0537(2)	0.114(11)	0.984(9)	17.0(10)	2.8(7)	2.13(40)
	4.63(18)	0.7731(24)	0.0890(33)	0.199(11)	0.986(6)	13.8(8)	3.9(9)	1.77(23)
	5.97(12)	0.777(17)	0.1232(37)	0.268(10)	0.988(6)	11.2(12)	5.5(6)	1.65(13)
	7.58(31)	0.783(8)	0.172(11)	0.339(11)	0.986(7)	8.5(18)	6.0(15)	1.49(8)
	8.53(42)	0.782(7)	0.212(16)	0.439(43)	0.986(5)	5.6(9)	7.7(18)	1.33(27)
	9.63(26)	0.774(12)	0.266(9)	0.529(12)	0.985(5)	3.6(20)	8.1(16)	1.23(8)
363.2	1.63(11)	0.7273(14)	0.0252(10)	0.038(5)	0.891(25)	18.2(21)	0.8(1)	2.04(39)
	2.07(26)	0.7275(13)	0.0324(38)	0.058(8)	0.926(13)	17.3(25)	1.0(1)	1.90(24)
	3.75(11)	0.7333(38)	0.0613(18)	0.116(6)	0.956(15)	14.6(18)	2.0(4)	1.78(21)
	5.94(17)	0.7331(13)	0.1050(36)	0.190(6)	0.964(9)	11.4(16)	3.0(5)	1.63(29)
	7.80(16)	0.737(10)	0.1460(49)	0.255(11)	0.965(8)	8.2(19)	4.0(9)	1.51(10)
	9.48(28)	0.733(8)	0.1860(40)	0.345(10)	0.969(7)	6.3(14)	5.2(8)	1.40(12)
	11.38(43)	0.728(18)	0.251(12)	0.423(19)	0.960(7)	4.0(10)	4.8(12)	1.25(18)

Nomenclature

Abbreviations

CO_2	carbon dioxide
DGT	density gradient theory
EtOH	ethanol
EOS	equation of state
LRC	long–range correction
MD	molecular dynamics
PC–SAFT	perturbed chain statistical associating fluid theory
PDM	pendant drop method

Latin symbols

E_{CO_2}	enrichment of carbon dioxide (1);
f_{CO_2}	fugacity of carbon dioxide (Pa)
g	acceleration constant (m s^{-2})
k_B	Boltzmann constant (J K^{-1})
k_{ij}	binary parameter in the PC–SAFT equation of state (1)
m	segment number in the PC–SAFT equation of state (1)
N	number of particles (1)
p	pressure (Pa)
q	point charge (C)
Q	quadrupole moment (C m^2)
r	site–site distance (m)
R	radius of curvature (m)
S	interfacial area (m^2)
t	time (s)
T	temperature (K)
x	mole fraction (1)
y	length coordinate (m)
z	drop height (m)

Greek symbols

γ	interfacial tension (N m^{-1})
$\Gamma_{CO_2}^{(EtOH)}$	relative adsorption of carbon dioxide with respect to ethanol (mol m^{-2})
$\Delta\rho$	difference between the saturated liquid phase and vapor phase mass density (kg m^{-3})
$\Delta\Omega$	grand potential per volume (J m^{-3})
ε	Lennard–Jones energy parameter in the MD simulations and segment interaction energy in PC–SAFT (J)
ε^{AB}	association energy in the PC–SAFT equation of state (J)
κ_{ij}	influence parameter in density gradient theory (mol^2 J^{-1} m^{-5})
κ^{AB}	association volume in the PC–SAFT equation of state (1)
μ_i	chemical potential of component i (J mol^{-1})
ξ	binary interaction parameter of the Berthelot combining rule in MD simulations (1)
ρ	mass density (kg m^{-3}) or molar density (mol m^{-3})
$\boldsymbol{\rho}$	vector of the molar component densities (mol m^{-3})
σ	Lennard–Jones size parameter in MD simulations and segment diameter in PC–SAFT (m)
ϕ_{CO_2}	fugacity coefficient of carbon dioxide (1)

Superscripts

bulk	bulk phase
red	reduced
pure	pure component
$'$	liquid bulk phase at saturation
$''$	vapor bulk phase at saturation

Subscripts

apx	drop apex

i, j	component
ref	reference